Chapter 5

Structural and Vibrational Properties of C_{60} and C_{70} Fullerenes Encapsulating Carbon Nanotubes

Hassane Chadli, Fatima Fergani and Abdelali Rahmani

Additional information is available at the end of the chapter

http://dx.doi.org/10.5772/intechopen.71246

Abstract

Carbon nanotubes (CNTs) can encapsulate small and large molecules, including C_{60} and C_{70} fullerenes (so-called carbon peapods). The challenge for nanotechnology is to achieve perfect control of nanoscale-related properties, which requires correlating the parameters of synthesis process with the resulting nanostructure. For that purpose, note every conventional characterization technique is suitable, but Raman spectroscopy has already proven to be. First, the different possible configurations of C_{60} and C_{70} molecules inside CNTs are reviewed. Therefore, the following changes of properties of the empty nanotubes, such as phonon modes, induced by the C_{60} and C_{70} filling inside nanotube are presented. We also briefly review the concept of Raman spectroscopy technique that provides information on phonon modes in carbon nanopeapods. The dependencies of the Raman spectrum as a function of nanotube diameter and chirality, fullerene molecules configuration and the filling level are identified and discussed. The experimental Raman spectra of fullerenes and fullerenes peapods are discussed in the light of theoretical calculation results. Finally, the variation of the average intensity ratio between C_{60} and C_{70} Raman-active modes and the nanotube ones, as a function of the concentration molecules, are analyzed, and a general good agreement is found between calculations and measurements.

Keywords: fullerene, C_{60}, C_{70}, carbon nanotubes, peapods, Raman spectroscopy

1. Introduction

Since Kroto *et al.* discovered C_{60} by laser vaporizing graphite into a helium stream in September 1985, fullerenes are at the heart of nanotechnology [1]. Other fullerenes were discovered shortly afterward with more and fewer carbon atoms. Since the discovery of multiwalled carbon nanotubes and single-walled carbon nanotube (SWCNT) in 1991 [2, 3], fullerenes and

carbon nanotube systems have attracted significant attention from the scientific community. A remarkable property of SWCNT is its ability to have been filled with various fullerenes and metallofullerenes, fullerenes adducts, metal complexes, and other small molecules. These fillings are highly dependent on the nanotube diameter and the inserted molecule size, so that even small changes in SWCNT diameter can alter the geometry of fullerene arrays. This class of hybrid materials has been dubbed as "peapods" (C_{60}@SWCNT and C_{70}@SWCNT), reflecting structural similarities to real peapods. After the discovery of C_{60} peapods by Smith et al. in 1998 [4], many experimental studies clearly evidenced the existence of various fullerenes like C_{70}, C_{76}, and C_{80} inside SWCNTs [5–7]. However, these materials represent a new class of a hybrid system between fullerenes and SWCNTs where the encapsulated molecules peas and the SWCNT pod are bonded through van der Waals interactions. Using high-resolution transmission electron microscopy (HR-TEM) experiments, the peapods are clearly observed, as seen in **Figure 1**, and organized into bundles [6–8].

The physicochemical properties of the fullerene molecules inserted inside carbon nanotubes are generally well known in their stable phase. But what happened when these same molecules are confined inside a carbon nanotube? Furthermore, changes in the electronic and mechanical properties of carbon nanotubes induced by the insertion of these molecules have been demonstrated [9, 10]. Peapods are typically characterized by one or more of the conventional techniques such as transmission electron microscopy (TEM), Raman spectroscopy, electron diffraction, electron energy loss spectroscopy (EELS), and X-ray diffraction. Raman spectroscopy is a useful tool to characterize carbon nanotubes and related nanomaterials and widely used by experimentalists as a fast and nondestructive method to identify the type of nanoparticle and to study their electronic and vibrational properties [11]. In this chapter, the structure and vibrational properties of C_{60} and C_{70} peapods are reviewed. We show that the structure of the

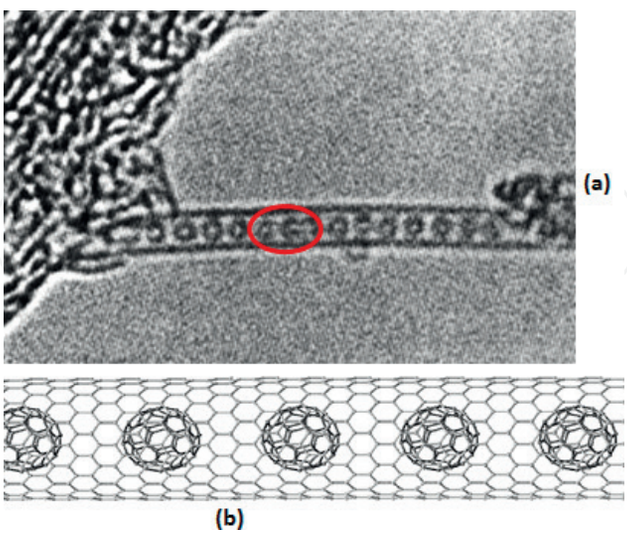

Figure 1. (a) Electron microscopy image of C_{60} peapod (from reference [4]). (b) Schematic representation of the molecular structure of an individual C_{60} peapod.

C_{60} and C_{70} molecules encapsulated inside SWCNTs adopt different configurations according to the nanotube diameter. Then, we report for each structure its associated calculated Raman responses. The dependencies of the Raman spectrum with different structural parameters such as nanotube diameter, fullerenes configuration, and the filling level are discussed. Finally, we evaluate, for each peapod configuration, the reliability and the transferability of the experimental method proposed by Kuzmany [12] to estimate the relative C_{60} and C_{70} concentrations in peapods.

2. Structure and dynamics of C_{60} and C_{70} peapods

2.1. Configuration of C_{60} and C_{70} inside carbon nanotubes

A C_{60} (C_{70}) carbon peapod is considered to be consisting of a number of C_{60} (C_{70}) molecules inside SWCNT. The configurations of C_{60} and C_{70} molecules within nanotube are diameter dependent. Carbon peapods can be produced in a very high yield close to 90% simultaneously by heating opened SWCNTs and fullerenes in a scaled quartz tube [6] and by the vapor phase reaction by using open end SWCNTs [7, 8]. The encapsulated molecules peas and the SWCNT pod are bonded through van der Waals interactions [6].

2.1.1. C_{60} peapods

Several theoretical and experimental studies have been reported on C_{60} formed within SWCNTs, and several interesting structural properties have been predicted or observed. In particular, theoretical calculations of C_{60} peapods suggest that the smallest tube diameter for encasing C_{60} molecules inside SWCNT is around the diameter corresponding to (10,10) or (9,9) SWCNTs [7]. Hodak and Girifalco showed that the guest molecules structure within the nanotube is diameter dependent [13, 14]. Using a convenient Lennard-Jones expression of the van der Waals intermolecular potential to derive the optimum configurations of C_{60} molecules inside single wall carbon nanotubes, Chadli et al. have found that the C_{60} molecules adopt a linear configuration with SWCNT diameters below 1.45 nm and a zigzag configuration for SWCNT diameters between 1.45 and 2.20 nm [15–17] (see **Table 1**). The optimum C_{60} packing can be characterized by the angle formed by three consecutive C_{60} (see **Figure 2a**). This angle θ is found to depend primarily on the nanotube diameter and does not depend significantly on the nanotube chirality. In the following paragraphs, the peapods in which the C_{60} molecules adopt a linear (zigzag) configuration are called linear (zigzag) peapods.

The calculations of structural parameters of C_{60} peapods are extended to a larger range of nanotube diameters in which C_{60} molecules can adopt a double helix (**Figure 2b**) or a two-molecule layer (**Figure 2c**) configuration. When the tube diameter increases up to 2.28 nm, the energy minimizations show that two other optimal configurations of C_{60} molecules are possible: a double helix structure ($2.15 \leq D \leq 2.23$ nm) and a two-molecule layer ($2.23 \leq D \leq 2.28$ nm). Optimized structural parameters issued from the energy minimizations are listed in **Table 2**.

Tube index (n,m)	Diameter (nm)	C60-tube distance (nm)	Angle θ (deg)	C60-C60 distance (nm)
(10,10)	1.36	0.323	180	1.003
(15,4)	1.41	0.355	180	1.003
(11,11)	1.49	0.321	164	1.006
(18,4)	1.59	0.309	150	1.003
(12,12)	1.63	0.306	145	1.008
(21,0)	1.64	0.307	143	1.008
(15,10)	1.70	0.30	134	1.006
(22,0)	1.72	0.302	132	1.006
(13,13)	1.76	0.301	127	1.007
(23,0)	1.80	0.30	121	1.003
(18,9)	1.86	0.298	112	1.003
(14,14)	1.90	0.30	108	1.006
(25,0)	1.96	0.298	99	1.006
(19,10)	2.00	0.298	90	1.008
(15,15)	2.03	0.3025	88	1.004
(17,14)	2.11	0.296	70	0.998

Table 1. Optimized linear and zigzag structural parameters of the C_{60} molecules inside SCNTs for different nanotubes diameter and chirality.

The optimal interlayer C_{60}-SWCNT distance is calculated around 0.30–0.33 nm, which is close to gaps commonly observed in carbon systems. For all optimized configurations, the interfullerene C_{60}-C_{60} distance varies from 0.998 to 1.01 nm. This result is in good agreement with the previously reported peapod interball separation of 0.97 nm from electron-diffraction profiles [18] and 0.95 nm from HRTEM data [7]. The predicted phases of C_{60}s inside SWCNTs have been experimentally observed by Kholoystov et al. HRTEM micrographs [19].

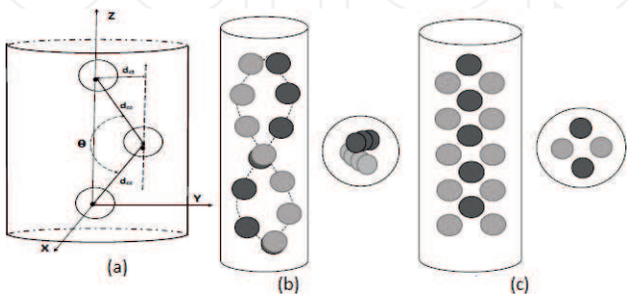

Figure 2. (a) Schematical representation of carbon peapods showing some of the parameters used for the geometrical optimization of the C_{60} molecules inside the nanotube (see text). (b) and (c) Schematic view of ordered phases resulting from C_{60} packing in SWCNTs: (b) double helix and (c) two-molecule layers.

C60 phases	Tube index (n,m)	Tube diameter (nm)	C60: tube distance (nm)	C60 – C60 Distance (nm)
Double helix	(22,9)	2.164	0.321	1.003
	(16,16)	2.171	0.323	1.001
	(18,14)	2.176	0.325	0.998
	(25,5)	2.181	0.323	1.001
	(19,13)	2.183	0.329	0.998
	(28,0)	2.193	0.331	1.001
	(27,2)	2.197	0.312	1.003
	(24,7)	2.206	0.309	1.003
	(26,4)	2.210	0.308	1.006
	(22,10)	2.221	0.30	1.008
Two molecule layers	(28,1)	2.233	0.312	1.01
	(17,16)	2.239	0.297	1.002
	(18,15)	2.242	0.302	1.008
	(19,14)	2.247	0.308	1.005
	(20,13)	2.255	0.306	1.006
	(24,8)	2.259	0.307	1.008
	(21,12)	2.266	0.311	1.01
	(29,0)	2.271	0.303	1.007
	(28,2)	2.276	0.308	1.009
	(22,11)	2.280	0.310	1.01

Table 2. Packing phases parameters obtained from minimized energy of the C_{60} molecules inside SCNT with diameters between 2.16 and 2.28 nm.

2.1.2. C_{70} peapods

Fullerenes with ellipsoidal shape-like C_{70} are of particular interest. Unlike the spheroidal molecules such as C_{60}, there are several geometrically distinct orientations possible for the C_{70} molecule within a nanotube. Experimentally, depending on the nanotube diameter, two different orientations (with regard to the nanotube axis) of a C_{70} molecule encapsulated into SWCNTs are observed by Chorro et al.: the lying down orientation where the long axis of C_{70} molecules is parallel to the nanotube long axis, and the standing up orientation where the C_{70} long axis is perpendicular to the nanotube axis [19, 20]. The value of the nanotube diameter beyond which the change from the lying to standing orientation occurs is experimentally estimated to ~1.42 nm. Besides, HRTEM measurements showed that there is no SWCNT containing C_{70} in both orientations.

These results indicate that only one type of orientation can exist for a given nanotube and confirm that the C_{70} alignment is associated with the geometrical parameters of the nanotube host. Theoretical studies showed that the configuration of C_{70}s inside SWCNT depends primarily on tube diameter and does not significantly depend on tube chirality [21, 22]. In order to obtain the optimal structure of the C_{70} inside the nanotubes, an energy minimization procedure was performed by Fegani et al. (for more detail, see reference [21]). The authors found that the C_{70} molecules adopt a lying orientation for small SWCNT diameters (below 1.356 nm), whereas a standing orientation is preferred for large diameters (above 1.463 nm). Between these diameters, an intermediate tilted regime where C_{70} are tilted have been obtained (see **Figure 3**).

Structural parameters issued from the energy minimization are listed in **Table 3**. The optimum fullerene packing can be characterized by the inclination θ of the molecule long axis with respect to the nanotube axis: θ = 0° for lying orientation, θ = 90° for standing orientation, and 0° < θ < 90° for tilted orientation.

2.2. Elements of lattice dynamics

An extensive review on phonon dynamics is out of the scope of this chapter. The lattice dynamical properties comprise the phonon modes, which provide fundamental information regarding the interatomic interaction within the material, and direct connections can be made to macroscopic phenomena and properties. The lattice dynamics theory was established by Born in the 1920s and further developed by Debye, Einstein, and others. For a comprehensive description and discussion regarding lattice dynamic theory, readers are referred to the book by Born and Huang [23]. We restrict the presentation to vibrations within the harmonic approximation. In this case, the expression of the hamiltonianis:

$$H = \frac{1}{2}\sum_{i\alpha} M_i \dot{u}_\alpha (i)^2 + \varnothing \tag{1}$$

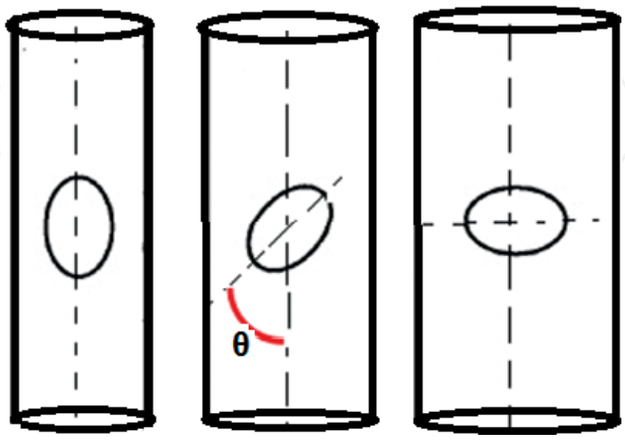

Figure 3. Orientations of a C_{70} inside a SWCNT: (a) lying, (b) tilted, and (c) standing.

SWNT index (n,m)	SWNT diameter (nm)	C_{70}-SWNT distance (nm)	Angle θ (deg)	C_{70}-C_{70} distance (nm)
(17,0)	1.330	0.307	0	1.125
(14,5)	1.335	0.309	0	1.125
(10,10)	1.356	0.320	0	1.125
(18,0)	1.409	0.307	5	1.122
(17,2)	1.415	0.305	9	1.118
(12,9)	1.428	0.307	41	1.106
(13,8)	1.437	0.309	47	1.101
(17,3)	1.463	0.323	60	1.082
(19,0)	1.487	0.329	90	1.003
(16,5)	1.487	0.329	90	1.003
(11,11)	1.491	0.331	90	1.003

Table 3. Optimized structural parameters of the C_{70} molecules inside SCNT for different diameters and chiralities.

where $\varnothing$ is the potential energy of particles in interaction, while $u_\alpha(i)$ is the displacement of atom i. It is given by:

$$\varnothing = \varnothing_0 + \frac{1}{2}\sum_{ij,\alpha\beta} \varnothing_{\alpha\beta}(i,j)\, u_\alpha(i)\, u_\beta(j) \tag{2}$$

$\varnothing_0$ is the static potential energy of the system (molecule or crystal). The starting point is the calculation of the dynamical matrix D given by:

$$D_{\alpha\beta}(i,j) = \frac{1}{\sqrt{M_i M_j}} \varnothing_{\alpha\beta}(i,j) \tag{3}$$

where $\varnothing_{\alpha\beta}(i,j)$ are the force constants between i and j atoms, the mass M_i (M_j) of the $i(j)^{th}$atom. The symmetry of the system permits to reduce the number of independent $\varnothing_{\alpha\beta}(i,j)$ coefficients.

The dynamical matrix is the key component for the computation of accurate vibrational frequencies and normal modes and contains all the information required for vibrational analysis within the harmonic approximation. In the case of C_{60} and C_{70} peapods, the dynamical matrix is calculated by block by using the coupling between the density functional theory (C_{60} and C_{70}), Saito force field (SWCNT) [24], and van der Waals potential (fullerene − SWCNT and fullerene-fullerene interactions) type:

$$V_{LJ}(r) = 4\epsilon\left[\left(\frac{\sigma}{r}\right)^{12} - \left(\frac{\sigma}{r}\right)^{6}\right] \tag{4}$$

where the depth of the potential well and the finite distance at which the interparticle potential is zero are given by $\epsilon = 2.964$ meV and $\sigma = 0.3407$ nm, respectively.

3. Nonresonant Raman spectra: Model and method

3.1. Raman scattering

Raman scattering from molecules and crystals was treated by many authors, among them Long [25] and Turell [26]. The main origin of the scattered light is considered to be an electric oscillating dipole, P, induced in the medium (molecules, amorphous materials, glasses, and crystals), by the electromagnetic incident field E. At first order, the induced dipole moment is given by

$$\mathbf{P} = \tilde{\alpha}\mathbf{E} \tag{5}$$

where $\tilde{\alpha}$ is the electronic polarizability tensor.

In a Raman experiment (**Figure 4**), a visible, or near infrared light, of frequencyω_1, wave vector k_1, polarization unit vector e_1, is incident in an isotropic medium, (ε_0 is the dielectric constant of vacuum, c is the speed of light in vacuum, and η_1 is the indice of refraction of the medium at the laser frequency).

The time-averaged power flux of the Raman-scattered light in a given direction, with a frequency between ω_f and $\omega_f + d\omega_f$ in a solid angledΩ, is related to the differential scattering cross section,

$$\frac{d^2\sigma}{d\Omega d\,\omega_d} = \frac{\hbar\omega_d^2}{8\pi^2 c^4}\,\omega_i\,\omega_d^3[n(\omega)+1]\sum_{\alpha\beta\gamma\lambda} e_{2\alpha}e_{2\beta}I_{\alpha\gamma\beta\lambda}(\omega)\,e_{1\gamma}\,e_{1\lambda}, \tag{6}$$

where

$$I_{\alpha\gamma\beta\lambda}(\omega) = \sum_j a^*_{\alpha\gamma}(j)\,a_{\beta\lambda}(j)\frac{1}{2\omega_j}\left(\delta(\omega-\omega_j)-\delta(\omega+\omega_j)\right), \tag{7}$$

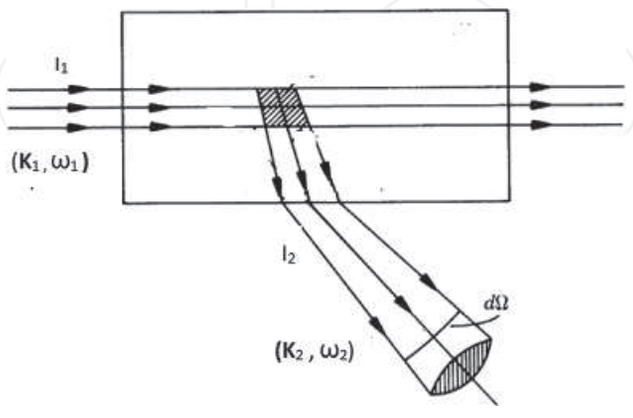

Figure 4. Sketch of a Raman scattering experiment.

n(ω) is the Bose factor, the Raman shift ω is $\omega = \omega_i - \omega_d$ and

$$a_{\alpha\gamma}(j) = \sum_{k\delta} \frac{\pi^k_{\alpha\gamma,\delta}}{\sqrt{M_k}} e_\delta(j \mid k) \tag{8}$$

where M_k the mass of the k^{th} atom, ω_j and $e_\delta(j \mid k)$ are the frequency and (δj) component of the j^{th} mode. The coefficients $\pi^k_{\alpha\gamma,\delta}$ connect the polarization fluctuations to the atomic motions. They are obtained by expanding the atomic polarizability tensor $\breve{\pi}^k$ in terms of atom displacementsu^k_δ, with

$$\pi^k_{\alpha\gamma,\delta} = \sum_{k'} \left(\frac{\partial \pi^k_{\alpha\gamma}}{\partial u_\delta(k)}\right)_0 \tag{9}$$

$a_{\alpha\gamma}(j)$ is the $\alpha\gamma$ component of the so-called Raman polarizability tensor of the j^{th} mode, and ω_j is the frequency of the j^{th} vibration mode.

3.2. The bond polarizability model

The Raman intensities can be calculated within the framework of the nonresonant bond polarizability model [27]. The basic assumption of the bond polarizability model is that the optical dielectric susceptibility of the material or molecule can be decomposed into individual contributions, arising only from the polarizability α^b_{ij} of bonds b between nearest neighbor atoms. In this model, each bond is characterized by a longitudinal polarizability, α_l, and a polarizability perpendicular to the bond, α_p. Thus, the polarizability contribution of a particular bond b can be written as follows:

$$\pi^b_{ij}(r) = \frac{1}{3}\left(\alpha_l + 2\,\alpha_p\right)\delta_{ij} + \left(\alpha_l - \alpha_p\right)\left(\boldsymbol{r}_i \mathbf{r}_j - \frac{1}{3}\delta_{ij}\right), \tag{10}$$

where i and j are the Cartesian directions (x, y, z) and $\boldsymbol{r}$ is the unit vector along the bond b which connects the atom n and the atom m covalently bonded. Within this approach, one can assume that the bond polarizability parameters are functions of the bond lengths r only. The derivatives of Eq. (10) with respect to the atomic displamcent of the atom n in the direction k, $\pi^n_{ij,k}$, are linked to the Raman susceptibility of modes (see [27] for the detailed formalism) and are given by:

$$\pi^n_{ij,k} = \sum_m \frac{1}{3}\left(\alpha'_l + 2\alpha'_p\right)\delta_{ij}\boldsymbol{r}_k + \left(\alpha'_l - \alpha'_p\right)\left(\boldsymbol{r}_i \mathbf{r}_j - \frac{1}{3}\delta_{ij}\right)\boldsymbol{r}_k + \frac{\alpha_l - \alpha_p}{r}\left(\delta_{ik}\mathbf{r}_j + \delta_{jk}\boldsymbol{r}_i - 2\,\boldsymbol{r}_i \mathbf{r}_j \mathbf{r}_k\right) \tag{11}$$

where $\alpha'_l = \left(\frac{\partial \alpha_l}{\partial r}\right)_{r=r0}$, $\alpha'_p = \left(\frac{\partial \alpha_p}{\partial r}\right)_{r=r0}$ and r_0 is the equilibrium bond distance. The values of these parameters (α') are usually fitted with respect to the experiments. For example, in the case of the C_{60}, the sum over bonds in Eq. 11 includes two types of bonds, single and double, so there is one parameter that determines the Raman intensities for SWCNT.

3.3. The spectral moment's method

The direct method to calculate the Raman spectrum requires, besides the polarization parameters, direct diagonalization of the dynamical matrix to obtain the eigenvalues and the eigenvectors of the system. The diagonalization fails or requires long computing time when the system contains a large number of atoms, as for a long C_{60} and C_{70} chains inside nanotubes. By contrast, the spectral moment's method allows computing directly the Raman responses of harmonic systems without any diagonalization of the dynamical matrix [28, 29]. In the case of C_{60} and C_{70} peapods, calculations of the Raman spectra of peapods showed that approximately 500 moments are sufficient to obtain good results for larger samples (~25,000 degrees of freedom).

4. Raman spectroscopy of C_{60} and C_{70} peapods

4.1. Raman-active modes in C_{60} and C_{70} fullerene

Because of their structural and vibrational properties, a lot of theoretical and experimental studies have been presented on C_{60} and C_{70} fullerenes, and several interesting properties have been predicted or observed. In particular, experimentalists have reported Raman scattering spectra of C_{60} and C_{70} measured by depositing fullerenes on the electrode or metal surface in order to obtain more intensive and more distinguishable spectral signals [30–32]. The free C_{60} and C_{70} cluster belongs to the Ih and D5h symmetry group, respectively. According to group theory [33, 34], the high symmetry of C_{60} gives rise to 10 Raman-active modes ($8H_g \oplus 2A_g$), while C_{70} has 53 Raman-active vibrational modes decomposed ($12A_1' \oplus 22E_2' \oplus 19E_1''$).

A large variety of theoretical methods have been applied to the calculation of C_{60} and C_{70} vibration of the internal modes and to the determination of their Raman activity. These approaches can be mainly classified as force field model [35, 36], modified neglect of diatomic overlap (MNDO) [37], Quantum-mechanical Consistent Force Field Method for Pi-Electron Systems (QCFF/PI) [38], and density functional theory [39]. The experimental and calculated frequency (cm^{-1}) of Raman-active modes in free C_{70} molecule with their assignments is listed in **Table 4**.

4.2. Raman spectra of carbon nanotubes

Raman spectroscopy is one of the primary methods used to yield the geometrical structure of one isolated individual SWCNT [40] and organized into bundles [11]. The experimental Raman spectra of SWCNTs are dominated by the radial breathing mode (RBM), the D-band, the G-band, and the G′-band (see **Figure 1** in [40]).

The fundamental two Raman-active modes are the RBM below 350 cm^{-1} and the tangential mode (TM) located between 1400 and 1600 cm^{-1}. The RBM is an important mode for the characterization and identification of specific nanotubes, in particular of their chirality. Recently, experimental and theoretical Raman studies have shown that the RBM frequency

Experiment				Calculation		Assignment
Ref [53]	Ref [54]	Ref [55]	Ref [56]	Ref [57]	Ref [21]	
226	228		233	219	218	E_2'
251			250	245	243	E1″
259	258	261	257	253	252	A1′
396	399	400	396	393	391	A1′
410	409	411	410	408	409	E1″
455	455	459	452	448	451	A1′
506	508	501	506	502	503	E2′
568	569	573	569	564	565	A1′
701	701	704	701	701	704	A1′
713	714		714	713	708	E1″
736	737	739	738	734	739	E2′
768	766	770	769	750	749	E2′
1060	1062	1062	1060	1060	1067	A1′
1182	1182	1186		1185	1186	A1′
				1186	1193	E2′
1227	1227	1231	1227	1229	1237	A1′
1257	1257	1260	1256	1256	1253	E2′
1296	1296	1298	1296	1296	1298	E1″
	1313	1317	1311	1312	1306	E1″
1331	1335	1336	1333	1328	1325	E2′
1367	1370	1370	1366	1366	1359	E1″
1467	1469	1471	1468	1471	1473	A1′
1494	1493			1501	1501	E2′
1511	1515	1517	1512	1515	1512	E1″
1564	1565	1569	1566	1574	1583	A1′

Table 4. Experimental and calculated frequency (cm^{-1}) of Raman-active modes in C_{70} fullerene with their assignments.

vs. diameter (d) follow the phenomological law $\omega_{RBM} = \left(\frac{228}{d}\right)\sqrt{1 + C d^2}$ with $C = 0$ for isolated SWCNTs [65], and $C \neq 0$ for SWCNT packed in bundles (see [41] and references therein). In SWCNT bundles, the origin of the C term results from van der Waals interaction. The G-band which closely related to vibrations in all sp2 carbon materials is an intrinsic feature of a carbon nanotube. The Raman line shape of this band which depends on whether the nanotube is semiconducting or metallic allows distinguishing between both types. This band shows a

low- and high-frequency component associated to the vibrations along the circumferential direction (G−) and the G direction of the nanotube axis (G+), respectively. In both metallic and semiconducting nanotubes, the former component is found to be dependent on the diameter of a nanotube, while the latter does not exhibit this dependence [40]. In the Raman spectra of isolated semiconducting and metallic SWCNT, the D-band and G'-band features are both observed.

4.3. Raman experiments on C_{60} and C_{70} peapods

Raman spectroscopy was employed to further characterize the peapod samples and to obtain structural information on the inserted fullerene inside tubes. Many groups have performed the Raman experiments of filling SWCNTs with C_{60} or C_{70} molecules [12, 42–46] since the first synthesized by Smith et al. [4]. **Figure 5** presents two examples of peapod experimental Raman spectra, one for C_{60}@SWCNT and the other for C_{70}@SWCNT.

Usually, experimental Raman spectra have been obtained on an ensemble of peapods organized into bundles. Nevertheless, the analysis of these experimental results for bundles of C_{60} peapods [8, 44] leads to the well-established conclusion: the Peapod Radial Breathing-Like Mode (PRBLM) of the peapod having a tube diameter close to 1.37 nm was split into two components, downshifted and upshifted, respectively, with respect to the position of the RBM in empty SWCNT. The upshift was possibly assigned to the stress feeling by the tubes from the inside C_{60}. For diameters between 1.45 and 1.76 nm, a single PRBLM measured

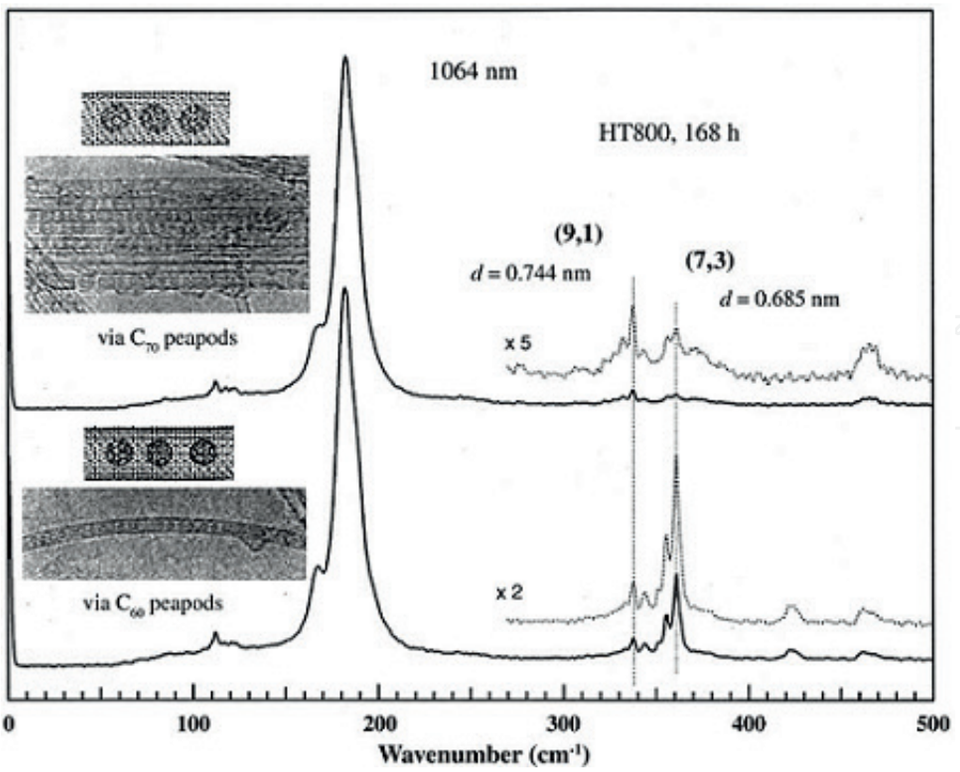

Figure 5. RBM Raman spectra taken for heat-treated C_{70} (top) and C_{60} (bottom) peapods (from reference [46]).

and its frequency are downshifted compared to the RBM in the empty SWCNT bundles. The observed downshift of the PRBLM [43, 44] is explained by the hybridization effect between SWCNTs and C_{60} molecules electronic states, leading to a decreasing of the electron density in the vicinity of the SWCNT, which induces a decreasing of the force constant of the C-C bond. Pfeiffer et al. [45] measured all the fundamental Raman lines of the encaged C_{60} peas. They observed that both nondegenerate and totally symmetric Ag modes of C_{60} peas exhibit a splitting into two components. They attributed this splitting to the presence of both moving and static fullerenes inside the tubes.

Kuzmany et al. [12] performed a detailed Raman analysis to evaluate the concentration of C_{60} molecules inside nanotubes. As expected, the relative concentrations derived from the measurement of normalized intensity ratio for each Raman mode of C_{60} are close. The C_{60} filling degree of a reference peapod sample was determined from electron energy loss spectroscopy experiment in order to evaluate the absolute C_{60} concentration of each peapod sample from the measurements of the Raman spectra (see **Table 1** of [12]).

Concerning the C_{70} peapods, Hirahara et al. [46] characterized one-dimensional crystals of a variety of larger fullerenes C_{70} peapods by using high-resolution transmission electron microscopy and electron diffraction. They concluded that the C_{70} admit two different orientations depending on the nanotube diameter: the lying and standing orientation. The intermolecular distances of various fullerenes in SWCNTs are considerably smaller than those for bulk fullerene crystals, suggesting an effect of confinement in the one-dimensional channels inside SWCNTs. Raman experiments on SWCNTs encasing C_{70} molecules have been reported [19, 21, 42, 47, 48]. Ryabenko et al. [42] concluded that the PRBLM mode of C_{70} peapods are downshifted by ~2–3 cm^{-1} compared to empty nanotubes. For different orientations of C_{70}s in C_{70}@SWCNT peapods organized into bundles, the measured PRBLM downshift after the C_{70} encapsulation is ~2–6 cm^{-1} [47]. The downshift of the PRBLM suggests a structural relaxation or the tube diameter transformation is expected to occur with the assistance of such added carbon atoms. However, such experimental work should include Raman investigations on samples showing peapods having various structural characteristics: different tube diameters, different fullerene concentration, and bundles with various sizes, for example, various numbers of tubes.

4.4. Raman-active modes calculation in C_{60} peapods

The Raman cross section was calculated assuming that scattering can be described within the framework of the bond polarizability model [52]. Recently, we calculated the Raman spectra of infinite homogeneous bundles (crystal) of C_{60} peapods [49]. In order to reach a 100% factor filling, 20 C_{60} molecules are located in a length of 19.8 nm [17.7 nm] of a (10,10) [(13,13)] nanotube and the number of carbon atoms of the tube (10,10) [(13,13)] is close of 3240 [3744] atoms. For the C_{60}@(10,10) (C_{60}@(13,13)) peapod, a 100% factor filling corresponds to a concentration of 37% (32%) (concentration is the ratio between carbons in C_{60} and carbons in the tube. In **Figure 6b** are displayed the calculated polarized ZZ Raman spectra of individual C_{60} peapods and crystal of C_{60} peapods, respectively, for linear and zigzag configuration of the C_{60} molecules inside the tube: (bottom) linear chain of

C_{60} confined into a (10,10) SWCNT (tube diameter close to 1.36 nm), (top) zigzag chain of C_{60} confined into a (13,13) SWCNT (tube diameter close to 1.76 nm).

In the intermediate and high-frequency regions, the calculated Raman spectra of individual peapods organized into infinite bundles do not show significant differences. It can be emphasized that a splitting of the Ag(1) and Ag(2) totally symmetric C_{60} modes was observed experimentally [45]. This splitting was considered as signature of the mobility of some encapsulated C_{60} molecules inside nanotubes [45]. In our calculations, the C_{60} molecules are kept at fixed positions in the considered peapods, and no splitting of the totally symmetric C_{60} modes is found.

Next, we show in **Figure 6b** the low-frequency range of Raman spectra of C_{60}@(10,10) and C_{60}@(13,13) peapods where the main changes are identified. We found that the PRBLM of individual C_{60}@(10,10) linear peapod on one hand and the PRBLM(1) and PRBLM(2) of individual C_{60}@(13,13) zigzag peapod on the other hand are slightly upshifted in bundles of C_{60}@(10,10) peapods and C_{60}@(13,13) peapods, respectively. We calculated a shift of the RBLM from 170 cm^{-1} in the individual C_{60}@(10,10) peapod to 186 cm^{-1} in the infinite bundle of C_{60}@(10,10) peapods. In the case of C_{60}@(13,13), the PRBLM(1) and PRBLM(2) doublet calculated

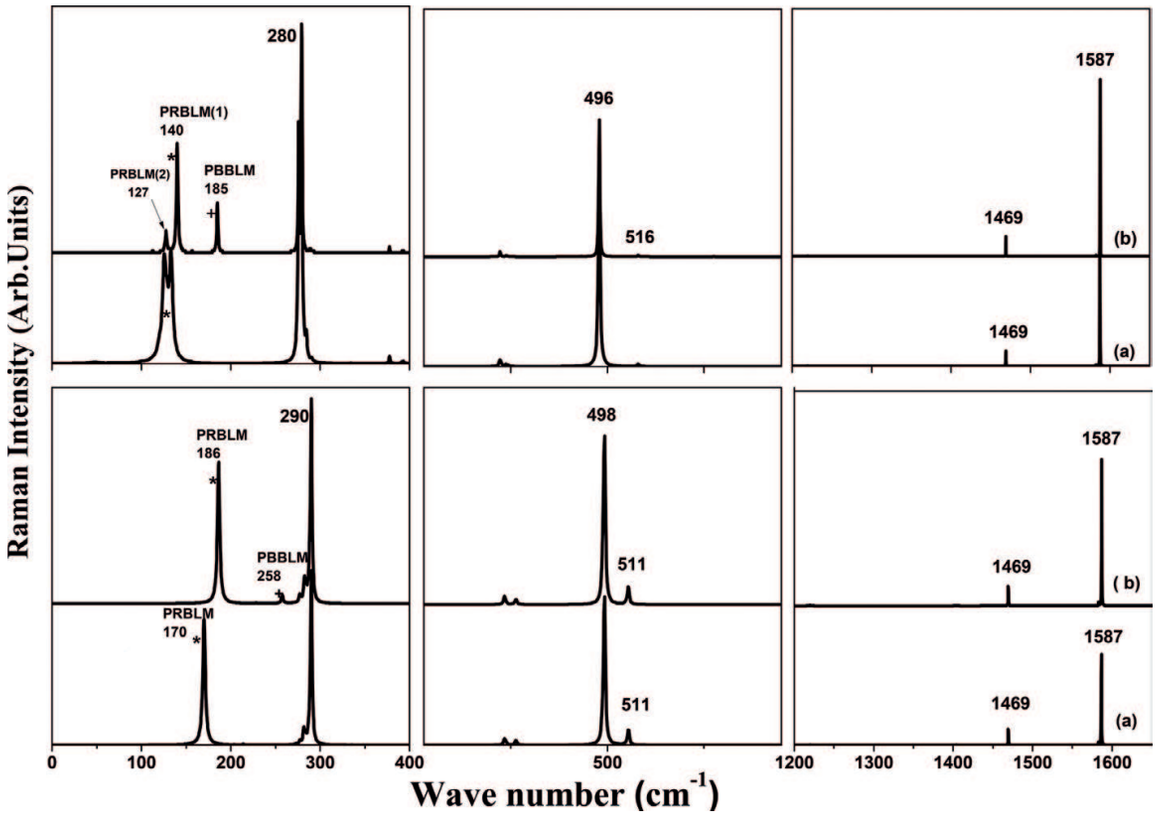

Figure 6. The ZZ calculated Raman spectra of individual (curve (a)) and homogeneous bundles (curve (b)) of C_{60}@(13,13) (top) and C_{60}@(10,10) (bottom) (filling factor 100%). The stars give the positions of the RBM and RBLM in individual SWCNT and crystal of SWCNT, respectively. Cross indicates the frequency of Bundle Breathing Like-Mode (BBLM) in crystal of SWCNT. (left) Breathing modes range, (middle) region of the radial C_{60} modes, (right) range of tangential modes: Ag(2) mode of C_{60} and G-modes of the nanotubes.

for the individual C_{60}@(13,13) peapod at 133 and 125 cm^{-1}, respectively, shifts to 140 and 127 cm^{-1} in the infinite bundle of C_{60}@(13,13) peapod. A new peapod bundle breathing-like mode (PBBLM) is also calculated in the Raman spectra of an infinite bundle of C_{60} peapods, which arises from the BBLM in SWCNT bundle [50]. Concerning the main Raman-active modes of C_{60} (e.g., modes located around 270 cm^{-1} (Hg) and 495 cm^{-1} (Ag)), independently of the configuration of C_{60} molecules inside the tube, the van der Waals interactions between peapods have no significant effect on these modes.

4.4.1. Diameter dependence of the Raman spectrum of C_{60} peapods

Figure 7 shows the PRBLM and PBBLM frequency dependencies as a function of the tube diameter. These dependencies are first compared with those of the RBLM and BBLM in unfilled bundles of tubes. The behavior of the PRBLM in linear peapods is qualitatively the same as those of RBLM in SWCNT bundle. However, the PRBLM frequency versus diameter relation deviates from the scaling law stated for the RBLM frequency in SWCNT bundle, especially for small diameters. For zigzag peapod, the PRBM(1) dependence as a function of the diameter is close to that of the RBLM in bundle of SWCNT. The PRBLM(1) downshifts when the tube diameter increases. Concerning the PBBLM frequency, it decreases with increasing the tube diameter and close to the frequency of BBLM, except at small diameters where a more significant increase of the PBBLM frequency is calculated. Our calculations based on DFT have clarified that the shift in the RBM frequencies of nanotubes containing fullerenes strongly depends on the diameters of the nanotubes. DFT calculations have also clarified that the shift in the RBM frequencies of nanotubes containing fullerenes strongly depends on the diameters of the nanotubes [51, 53–57].

More recently, Raman calculations are extended to a larger range of diameters in which C_{60} molecules can adopt a double helix and a layer of two molecules [22].

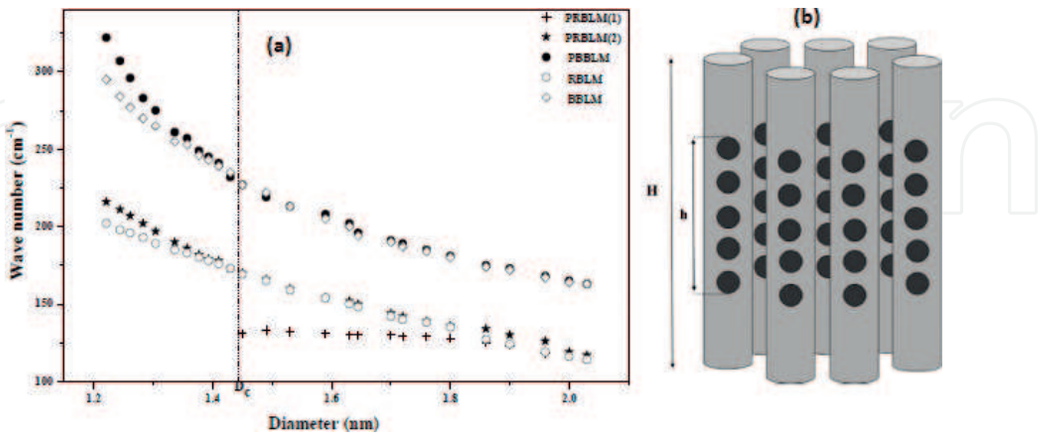

Figure 7. Diameter dependence of the frequencies of PRBLM (for d < Dc = 1.45 nm) and PRBLM(1) (for d > Dc) (stars), and PRBLM(2) (cross). Diameter dependence of the frequency of RBLM (open circles) and BBLM (open diamonds) in bundles of SWCNTs. The critical diameter Dc between linear (tube diameters lower than Dc) and zigzag (tube diameters greater than Dc) peapods is identified by the vertical-dashed line. (b) Schematic representation of homogeneous filling mode of the different tubes within a bundle. The filling factor is related to the ratio h/H (see text).

4.4.2. Filling rate effect

In real carbon peapod samples, it is reasonable to consider that all the nanotubes are not completely filled with fullerenes. The degree of filling ranges from a certain percent to almost 100% [6]. In the following paragraphs, we discuss the main features of the filling rate effect on both configurations of C_{60} inside SWCNT, double helix, and two-molecule layer. We assume that the molecules tend to cluster inside nanotubes. Indeed, this should correspond to a low energy configuration of the system as the energy is lowered by the attractive C_{60}-C_{60} interactions. The filling factor is defined as the number of carbon atoms of C_{60} molecules contained in the h length with regard to the number of carbon atoms contained in the H length of the host tube normalized with the concentration related to the filling factor of 100% (see **Figure 7b**). The calculated ZZ-polarized Raman spectra of the C_{60}@(28,0) (double helix chain of C_{60}) and C_{60}@(29,0) (two-molecule layer) peapods are reported in **Figure 8** as a function of five filling rates (20, 40, 60, 80, and 100%). Where the RBLM range is very sensitive to filling rate and the TLM range slightly depends on the degree of filling of the SWCNT, the TLM range is not shown.

For both configurations, a single PRBLM is predicted whatever the tube filling. For the empty tubes, the RBM is located at 102 and 98 cm^{-1} for the (28,0) and (29,0) SWCNTs, respectively. For a high filling level, it is upshifted at 103 and 100 cm^{-1} in the C_{60}@(28,0) and C_{60}@(29,0) peapods, respectively. As expected, the intensity of the Hg(1) line located at 270 cm^{-1} in C_{60} increases when the filling factor increases.

4.5. Calculation of Raman-active modes in C_{70} peapods

In this section, we review the theoretical Raman spectra of the C_{70} peapods calculated as a function of diameter and C_{70} filling rate. These calculations support the experimental

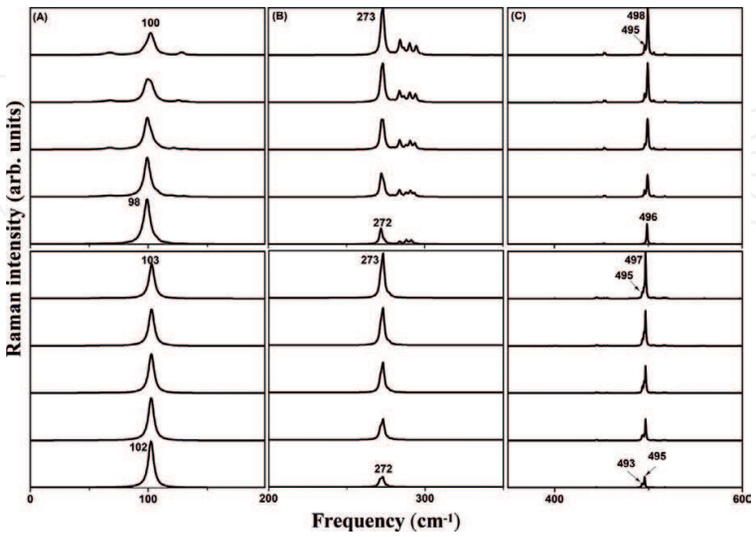

Figure 8. Calculated ZZ-polarized Raman spectra of C_{60}@(28,0) (bottom) and C_{60}@(29,0) (top) as a function of the filling rate and displayed in the BLM region. From bottom to top, the filling rate is: 20, 40, 60, 80, and 100%.

evidence on the C_{70} orientations as a function of the SWCNT diameters, and they address new questions as to the influence of the nanotube chirality and the C_{70} filling rate.

4.5.1. Diameter effects

In order to investigate how the frequency of the Raman-active mode in C_{70}@SWCNT changes when the C_{70} molecule adopts various orientations, and three zigzag SWCNTs have been considered with a diameter of 1.330 [(17,0)], 1.409 [(18,0)], and 1.487 nm [(19,0)] where C_{70} molecules adopt lying, tilted, and standing orientation, respectively. The calculated ZZ-polarized Raman spectra of C_{70} peapods are shown in **Figure 9** along with their corresponding unfilled nanotubes and the unoriented C_{70} molecule. Raman lines can be divided into three frequency ranges: (1) below 500 cm^{-1} where the breathing-like modes (BLM) dominate (panel A), (2) an intermediate range between 500 and 1500 cm^{-1} (panel B), and (3) above 1500 cm^{-1} where the tangential-like modes (TLM) are located (panel C).

In the TLM range, the main modes of SWCNT are almost not significantly sensitive to the orientation of C_{70} molecules inside the nanotube. In the intermediate range, the C_{70} spectrum is dominated by two strong lines at 1192 and 1253 cm^{-1}, while no Raman line is expected for SWCNTs. Thus, Raman spectra of peapods show several weak lines which originate from the splitting of the C_{70} degenerate modes due to van der Waals interactions. In this range, Raman spectra of peapods are dominated by two lines around 740 and 1272 cm^{-1}. A third line can also be identified at 1391 cm^{-1} for the standing orientation and at 1490 cm^{-1} for lying and tilted orientations.

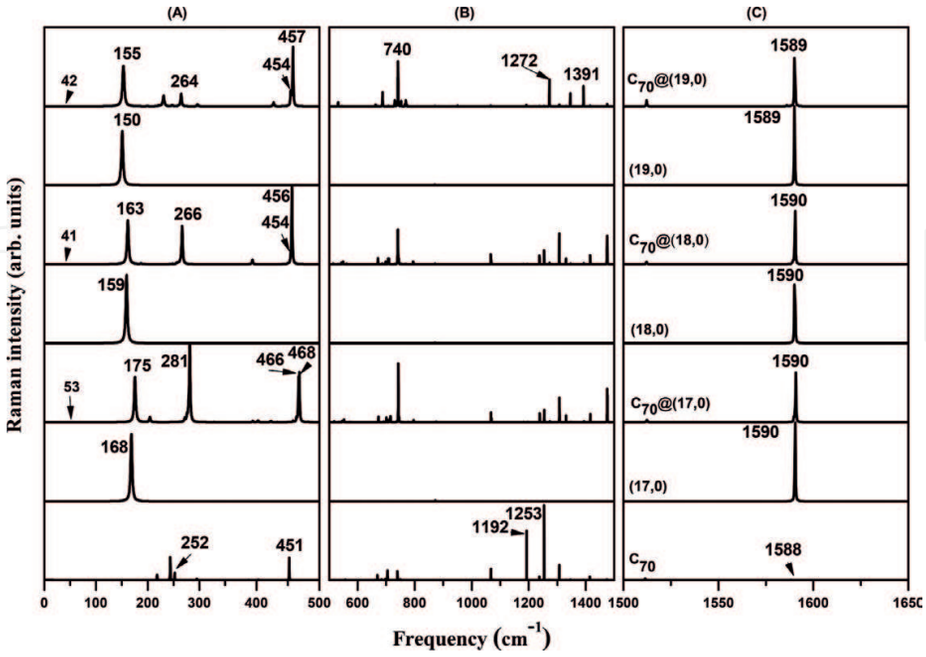

Figure 9. ZZ-calculated Raman spectra of C_{70} peapods along with their corresponding unfilled nanotubes and unoriented free C70 molecule. Spectra are displayed in the BLM (A), intermediate (B), and TLM (C) ranges.

4.5.2. Filling factor effects

To investigate the effect of incomplete filling rate on Raman spectra of C_{70} peapod, we considered three kinds of peapods: the C_{70}@(17,0) lying, C_{70}@(17,3) tilted, and C_{70}@(11,11) standing orientations. The spectra were calculated for five values of the filling factor F = 20, 40, 60, 80, and 100% corresponding to 2, 4, 8, 12, and 16 C_{70} molecules inside SWCNTs, respectively (see **Figure 10**). Periodic conditions were applied along the tube axis to avoid finite size effects.

As expected, the filling level of C_{70} molecules inside the SWCNTs has no significant effect on the Raman spectrum in the TLM range (not shown). In contrast, in the BLM range, the Raman spectra are quite sensitive to the filling factor: an upshift of approximately 2–5 cm^{-1} is obtained for the RBM modes in standing orientations when F increases up to 100%, whereas a splitting of these modes is observed in the lying and tilted orientations. This splitting is in agreement with experimental results of Bandow et al. [8]. For example, for lying orientation (small diameters), the increase of the filling factor from 0 to 100% leads to the appearance of two lines at frequencies close to 168 and 175 cm^{-1}. Their intensity shifts from the one located around 168 cm^{-1} to that located around 175 cm^{-1} as the filling factor increases.

4.6. Raman spectra analysis: C_{60} and C_{70} concentration determination in peapods

The evolution of the nonresonant Raman scattering intensity ratios between the Raman mode of fullerene peas and nanotubes as a function of the fullerene concentration inside the tubes has been investigated in the framework of the spectral moment's method [21, 50]. Although the nonresonant approach cannot predict the variation of the line intensities with the excitation energies, the obtained predictions are useful to follow their evolution as a function of the filling rate of fullerenes inside SWCNT. For this purpose, we performed an average of

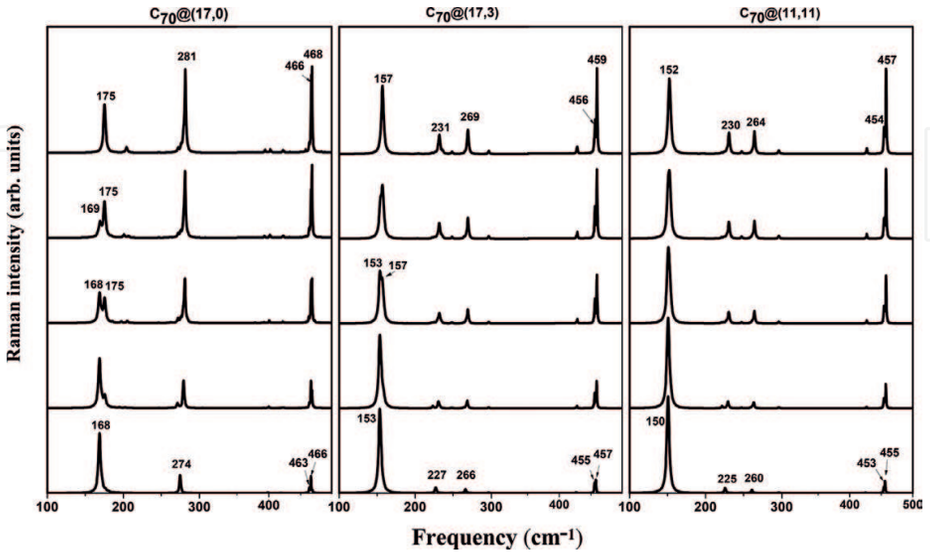

Figure 10. ZZ-polarized Raman spectra of infinite peapods displayed in the BLM region as a function of the filling factor: F = 20, 40, 60, 80, and 100% from bottom to up.

the Raman spectra over the peapod orientations with regard to the laboratory frame. Raman spectra are calculated in the VV configuration for unoriented peapod samples for various values of the fullerene filling factor. The relative intensity ratios have been calculated as a function of the C_{60} and C_{70} fullerenes concentrations.

First, for C_{60} peapod, we calculated the intensity ratio between the Raman lines of the C_{60} molecule [Hg(2), Ag(1), Hg(3), Hg(4), Hg(7), and Ag(2)] and the PRBLM or G-mode. In order to make the comparison with the experimental results of Kuzmany et al. [12], the calculated intensity ratio is normalized with respect to the same intensity ratio calculated for the 60% filling factor sample. The relative C_{60} concentrations that are derived according to this procedure are displayed in **Figure 11** for the C_{60}@(17,0), C_{60}@(22,0), C_{60}@(28,0), and C_{60}@(29,0) which correspond to linear, zigzag, double-helix, and two molecule layers chain of C_{60}, respectively. As expected, for all the investigated peapod diameters, the relative concentrations calculated for each C_{60} mode are close. The relative concentrations calculated for infinite peapods increase when its diameter increases. For instance, for a filling factor ~20%, the relative concentration is close to 0.21, 0.26, 0.3, and 0.4 for a diameter of 1.35 [C_{60}@(17,0)], 1.76 [C_{60}@(22,0)], 2.19 [C_{60}@(28,0)], and 2.27 nm [C_{60}@(29,0)], respectively. For a ~ 20% concentration (corresponding to the L43 sample (EELS concentration 25 ± 10) in [12]), the average relative concentration is

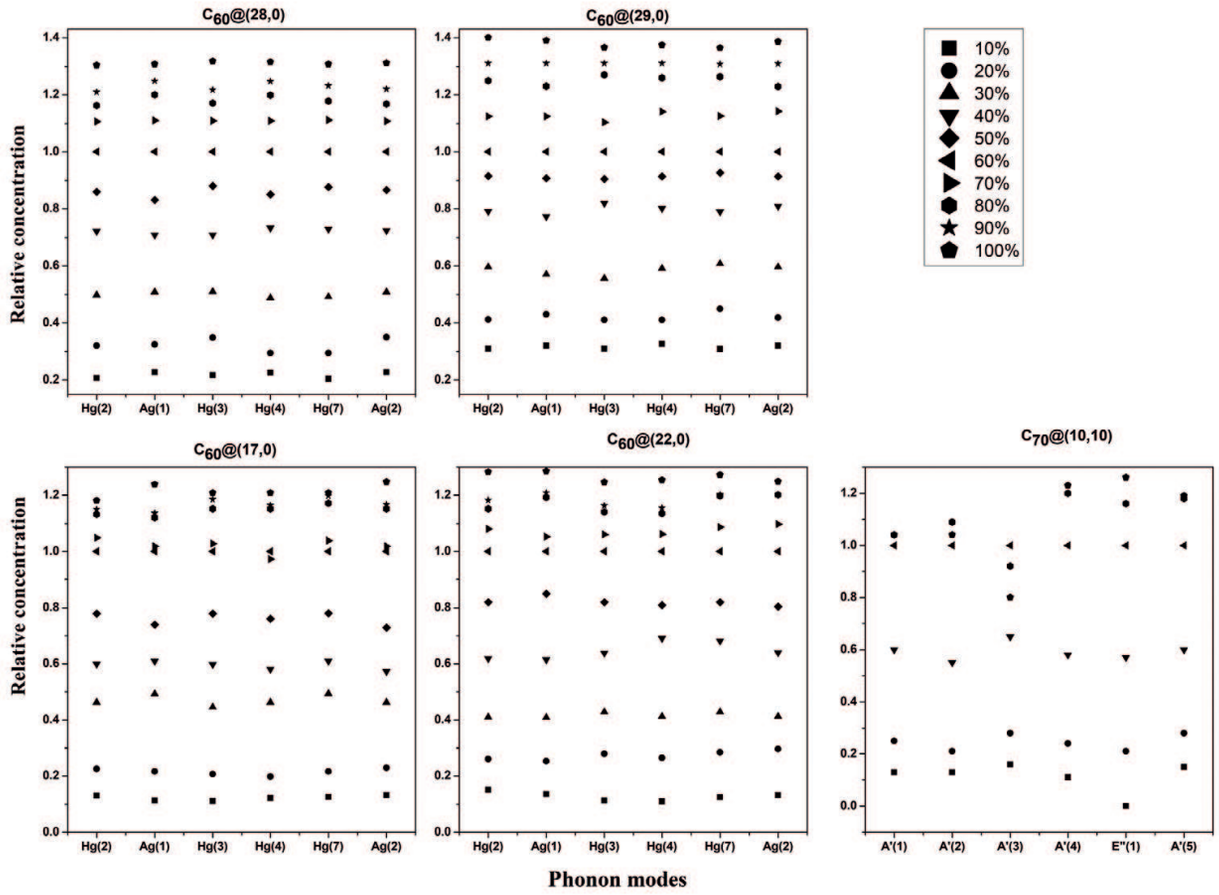

Figure 11. Relative concentration of several configurations of C_{60} inside SWCNTs and C_{70}@(10,10) normalized on the 60% filling rate intensities.

calculated around 0.21 ± 0.02, in good agreement with the experimental relative concentration evaluated around 0.19. This good agreement supports the experimental method proposed by Kuzmany et al. to evaluate C_{60} concentration inside SWCNTs.

Next, we calculate the integrated intensity ratios between the Raman lines of the C_{70} molecule [low-frequency modes located at: A1′: 252 cm^{-1} (A1′(1), A1′: 391 cm^{-1} (A1′(2)), A1′: 451 cm^{-1} (A1′(3)) and high-frequency Raman modes: A1′: 1473 cm^{-1} (A1′(4)), E1″: 1512 cm^{-1} (E1″(1)) and A1′: 1583 cm^{-1} (A1′(5))] and the PRBLM or G-mode. The relative concentrations derived by this way are shown in **Figure 11**. For a filling factor 20%, the relative concentration is close to 0.21 for C_{70} inside (10,10). The comparison of data of the relative concentration of C_{60} (linear chain) with those of C_{70} (lying orientation) shows qualitatively the same result.

5. Concluding remarks

In this chapter, we have discussed the optimal configurations of the C_{60} and C_{70} molecules inside SWCNTs. First, the configuration of C_{60} and C_{70} fullerenes inside SWCNT is found to depend strongly on the nanotube diameter and does not depend significantly on tube chirality. In agreement with experiments, the C_{70} molecules adopt a lying orientation for small SWCNT diameters (below 1.356 nm), whereas a standing orientation is preferred for large diameters (above 1.463 nm). Between these diameters, an intermediate tilted configuration of C_{70}s is found. For C_{60} peapods, C_{60}s adopt a linear arrangement for SWCNT diameter lower than 1.45 nm and a zigzag configuration for diameters between 1.45 and 2.15 nm. In the diameter range between 2.15 and 2.23 nm, C_{60} molecules adopt a double helix arrangement in SWCNTs, whereas a layer of two molecules is preferred for diameters between 2.23 and 2.28 nm. Next, we have reported the calculated Raman spectra of peapods. The modes located in the BLM range are very sensitive to the encapsulation of fullerenes because major changes in frequencies and intensities are observed. The average intensity ratios between C_{60} and C_{70} Raman-active modes and the nanotube ones, as a function of the concentration molecules, have been analyzed, and a general good agreement is found between calculations and measurements. This good agreement supports the experimental method proposed to evaluate C_{60} concentration inside SWCNTs.

Author details

Hassane Chadli[1], Fatima Fergani[2] and Abdelali Rahmani[2]*

*Address all correspondence to: a.rahmani@fs-umi.ac.ma

1 High School of Technology Khenifra - Moulay Ismail University, Meknes, Morocco

2 Laboratory of Advanced Materials Studies and Applications, Moulay Ismail University, FSM-ESTK-ESTM, Meknes, Morocco

References

[1] Kroto H, Heath J, O'Brien S, Curl R, Smalley R. Buckminsterfullerene. Nature. 1985;**318** (14):162-163. DOI: 10.1038/318162a0

[2] S. Ijima. Helical microtubules of graphitic carbon. Nature. 1991;**354**:56-58. DOI: 10.1038/354056a0

[3] Ijima S, Ichihachi T. Single-shell carbon nanotubes of 1-nm diameter. Nature. 1993;**363**: 603-605. DOI: 10.1038/363603a0

[4] Smith BW, Monthioux M, Luzzi DE. Encapsulated C_{60} in carbon nanotubes. Nature. 1998;**396**:323-324. DOI: 10.1038/24521

[5] Sloan J, Dunin-Borkowski RE, Hutchison JL, Coleman KS, Williams VC, Claridge JB, York APE, Xu C, Bailey SR, Brown G, Friedrichs S, Green MLH. The size distribution, imaging and obstructing properties of C_{60} and higher fullerenes formed within arc-grown single walled carbon nanotubes. Chemical Physics Letters. 2000;**316**:191

[6] Kataura H, Kumazawa Y, Maniwa Y, Umezu I, Suzuki S, Ohtsuka Y, Achiba Y. Highyield fullerene encapsulation in single-wall carbon nanotubes. Synthetic Metals. 2000;**121**:1195. DOI: 10.1016/S0379-6779(00)00707-4

[7] Hirahara K, Suenaga K, Bandow S, Kato H, Okazaki T, Shinohara H, Iijima S. One dimensional Metallofullerene crystal generated inside single-walled carbon nanotubes. Physical Review Letters. 2000;**85**:5384. DOI: 10.1103/PhysRevLett.85.5384

[8] Bandow S, Takizawa M, Kato H, Okazaki T, Shinohara H, Iijima S. Smallest limit of tube diameters for encasing of particular fullerenes determined by radial breathing mode Raman scattering. Chemical Physics Letters. 2001;**347**:23-28. DOI: 10.1016/S0009-2614(01)01020-X

[9] Hornbaker DJ, Kahng SJ, Misra S, Smith BW, Johnson AT, Mele ET, Luzzi DE, Yazdani A. Mapping on the one-dimensional electronic states of nanotube peapod structures. Science. 2002;**295**(5556):828-831. DOI: 10.1126/science.1068133

[10] Jaroenapibal P, Chikkannanavar SB, Luzzi DE, Evoy S. Nanomechanical resonance studies of carbon nanotube peapod bundles. The Journal of Applied Physics. 2005;**98**:044301. DOI: 10.1063/1.2001147

[11] Dressellhaus MS, Eklund PC. Phonons in carbon nanotubes. Advances in Physics. 2000;**49**(6):705-814. DOI: 10.1080/000187300413184

[12] Kuzmany H, Pfeiffer R, Kramberger C, Pichler T, Liu X, Knupfer M, Fink J, Kataura H, Achiba Y, Smith BW, Luzzi DE. Analysis of the concentration of C_{60} fullerenes in single wall carbon nanotubes. Applied Physics A: Materials Science & Processing. 2003;**76**:449. DOI: 10.1007/s00339-002-2046-8

[13] Hodak M, Girifalco LA. Ordered phases of fullerene molecules formed inside carbon nanotubes. Physical Review B. 2003;**67**:075419-075422. DOI: 10.1103/PhysRevB.67.075419

[14] Hodak M, Girifalco LA. Systems of C_{60} molecules inside (10,10) and (15,15) nanotube: A Monte Carlo study. Physical Review B. 2003;**68**:085405. DOI: 10.1103/PhysRevB.68.085405

[15] Chadli H, Rahmani A, Sbai K, Hermet P, Rols S, Sauvajol J-L. Calculation of Raman-active modes in linear and zigzag phases of fullerene peapods. Physical Review B. 2006;**74**:205412. DOI: 10.1103/PhysRevB.74.205412

[16] Chadli H, Rahmani A, Sbai K, Sauvajol J-L. Raman active modes in carbon peapods. Physica A: Statistical Mechanics and its Applications. 2005;**358**:226-236. DOI: 10.1016/j.physa.2005.06.025

[17] Chadli H, Rahmani A, Sauvajol J-L. Raman spectra of C_{60} dimer and C_{60} polymer confined inside a (10,10) single-walled carbon nanotube. Journal of Physics: Condensed Matter. 2010;**22**(14):145303. DOI: 10.1088/0953-8984/22/14/145303

[18] Liu X, Pichler T, Knupfer M, Golden MS, Fink J, Kataura H, Achiba Y, Hirahara K, Ijima S. Filling factors, structural, and electronic properties of C_{60} molecules in single-wall carbon nanotubes. Physical Review B. 2002;**65**:045419. DOI: 10.1103/PhysRevB.65.045419

[19] Khlobystov A N, Scipioni R, Nguyen-Manh D, Britz D A, Pettifor D G, Briggs G A D, Lyapin S G, Ardavan A, Nicholas R. Controlled orientation of ellipsoidal fullerene C_{70} in carbon nanotubes. The Journal of Applied Physics. 2004;**84**:792-794. DOI: 0003-6951/2004/84(5)/792/3/22.00

[20] Chorro M, Delhey A, No L, Monthioux M, Launois P. Orientation of C_{70} molecules in peapods as a function of the nanotube diameter. Physical Review B. 2007;**75**(3):035416. DOI: 10.1103/PhysRevB.75.035416

[21] Fergani F, Chadli H, Belhboub A, Hermet P, Rahmani A. Theoretical study of the Raman spectra of C_{70} fullerene carbon peapods. Journal of Physical Chemistry C. 2015;**119**:5679-5686. DOI: 10.1021/jp511969t

[22] Fergani F, Ait Abdelkader SA, Chadli H, Fakrach B, Rahmani AH, Hermet P, Rahmani A. C_{60} filling rate in carbon peapods: A nonresonant Raman spectra analysis. Journal of Nanomaterials. 2017;**2017**:1-7. DOI: 10.1155/2017/9248153

[23] Born M, Huang K. Dynamical Theory of Crystal Lattices. Oxford: Oxford University Press; 1954. p. 432. DOI: 10.1119/1.1934059

[24] Saito R, Takeya T, Kimura T, Dresselhaus G, Dresselhaus MS. Raman Intensity of Single-Wall Carbon Nanotubes. Physical Review B 545 1998, 57, 4145

[25] Long DA. The Raman Effect: A Unified Treatment of the Theory of Raman Scattering by Molecules. 2nd ed. Chichester: Wiley; 2011. p. 624. DOI: 10.1002/0470845767

[26] Turell G. Infrared and Raman spectra of crystals. London and New York: Academic Press; 1972. 384p. DOI: 10.1002/pol.1973.130110313

[27] Bilz, H., Strauch, D., Wehner, R.K. Light and Matter Id / Licht und Materie Id: Infrared and Raman Spectra of Non-Metals. vol. XXV. 1st ed. Handbuch der Physik. Berlin: Springer-Verlag; 1984, Pt. 2d, 253 p

[28] C. Benoit, E. Royer, G. Poussigue. The spectral moments method. Journal of Physics: Condensed Matter 1992;**4**:3125. DOI: 10.1088/0953-8984/4/12/010/meta

[29] Rahmani A, Sauvajol J-L, Rols S, Benoit C. Nonresonant Raman spectrum in infinite and finite single-wall carbon nanotubes. Physical Review B. 2002;**66**:125404. DOI: 10.1103/PhysRevB.66.125404

[30] Fredericks PM. Fourier transform surface-enhanced Raman scattering of C_{70} on a roughened silver surface. Chemical Physics Letters. 1996;**253**:251-256. DOI: 10.1016/0009-2614(96)00251-5

[31] Katayama N, Miyatake Y, Ozaki Y, Kikuchi K, Achiba Y, Ikemoto I, Iriyama K. Surface-enhanced Raman scattering (SERS) study of C_{60} and C_{70} in evaporated films by near-infrared FT-Raman spectroscopy. Proceedings of SPIE. 1994;**2089**:174-175. DOI: 10.1117/12.166755

[32] Luo ZX, Yan F. SERS of gold/C_{60}(/C_{70}) nano-clusters deposited on iron surface. Vibrational Spectroscopy. 2005;**39**:151-156. DOI: 10.1016/j.vibspec.2005.01.008

[33] Cotton FA. Chemical Applications of Group Theory. 3rd ed. New York: John Wiley & Sons. 1990. 461p. DOI: 10.1002/bbpc.19910950625

[34] Cyvin SJ, Brendsdal E, Cyvin BN, Brunvoll J. Molecular vibrations of footballene. Chemical Physics Letters. 1988;**143**(4):377-380. DOI: 10.1016/0009-2614(88)87050-7

[35] Jishi RA, Mirie RM, Dresselhaus MS. Force-constant model for the vibrational modes in C_{60}. Physical Review B. 1992;**45**(23):13685-13689. DOI: 10.1103/PhysRevB.45.13685

[36] Wu ZC, Jelski DA, George TF. Vibrational motions of buckminsterfullerene. Chemical Physics Letters. 1987;**137**(3):291-294. DOI: 10.1016/0009-2614(87)80221-X

[37] Stanton RE, Newton MD. Normal vibrational modes of buckminsterfullerene. The Journal of Physical Chemistry. 1988;**92**:2141-2145. DOI: 10.1021/j100319a012

[38] Negri F, Orlandi G, Zerbetto F. Quantum-chemical investigation of Franck Condon and Jahn–teller activity in the electronic spectra of buckminsterfullerene. Chemical Physics Letters. 1988;**144**(1):31-37. DOI: 10.1016/0009-2614(88)87084-2

[39] Weeks DE, Harter WG. Rotation-vibration spectra of icosahedral molecules. II. Icosahedral symmetry, vibrational eigenfrequencies, and normal modes of buckminsterfullerene. The Journal of Chemical Physics. 1989;**90**:4744-4771. DOI: 10.1063/1.456571

[40] Dresselhaus MS, Dresselhaus G, Jorio A, Souza Filho AG, Saito R. Raman spectroscopy on isolated single wall carbon nanotubes. Carbon. 2002;**40**(12):2043-2061. DOI: 10.1016/S0008-6223(02)00066-0

[41] Araujo PT, Maciel IO, Pesce PBC, Pimenta MA, Doorn SK, Qian H, Hartschuh A, Steiner M, Grigorian L, Hata K, Jorio A. Nature of the constant factor in the relation between radial breathing mode frequency and tube diameter for single-wall carbon nanotubes. Physical Review B. 2008;**77**:241403. DOI: 10.1103/PhysRevB.77.241403

[42] Ryabenko AG, Kiselev NA, Hutchison JL, Moroz TN, Bukalov SS, Mikhalitsyn LA, Loutfy RO, Moravsky AP. Spectral properties of single-walled carbon nanotubes encapsulating fullerenes. Carbon. 2007;**45**:1492-1505. DOI: 10.1016/j.carbon.2007.03.031

[43] Joung SK, Okazaki T, Kishi N, Okada S, Bandow S, Iijima S. Effect of fullerene encapsulation on radial vibrational breathing- mode frequencies of single-wall carbon nanotubes. Physical Review Letters. 2009;**103**:027403. DOI: 10.1103/PhysRevLett.103.027403

[44] Bandow S, Takizawa M, Hirahara K, Yudasaka M, Iijima S. Raman scattering study of doublewall carbon nanotubes derived from the chains of fullerenes in single wallcarbon nanotubes. Chemical Physics Letters. 2001;**337**:48-57. DOI: 10.1016/S0009-2614(01)00192-0

[45] Pfeiffer R, Kuzmany H, Pichler T, Kataura H, Achiba Y, Melle-Franco M, Zerbetto F. Electronic and mechanical coupling between guest and host in carbon peapods. Physical Review B. 2004;**69**:035404. DOI: 10.1103/PhysRevB.69.035404

[46] Bandow S, Hiraoka T, Yumura T, Hirahara K, Shinohara H, Iijima S. Raman scattering study on fullerene derived intermediates formed within single-wall carbon nanotube: From peapod to double-wall carbon nanotube. Chemical Physics Letters. 2004;**384**: 320-325. DOI: 10.1016/j.cplett.2003.12.032

[47] Guan L, Li H, Shi Z, You L, Gu Z. Standing or lying C_{70}s encapsulated in carbon nanotubes with different diameters. Solid State Communications. 2005;**133**:333-336. DOI: 10.1016/j.ssc.2004.11.008

[48] Kavan L, Dunsch L, Kataura H, Oshiyama A. Electro-chemical tuning of electronic structure of C_{60} and C_{70} fullerene peapods: In situ visible near-infrared and Raman study. The Journal of Physical Chemistry B. 2003;**107**(31):7666-7675. DOI: 10.1021/jp035332f

[49] Chadli H, Fergani F, Bentaleb M, Fakrach B, Sbai K, Rahmani A, Bantignies JL, Sauvajol JL. Influence of packing on the vibrations of homogeneous bundles of C_{60} peapods. Physica E: Low-dimensional Systems and Nanostructures. 2015;**71**:31-38. DOI: 10.1016/j.physe.2015.03.018

[50] Sbai K, Rahmani A, Chadli H, Sauvajol J-L. Raman-active modes in homogeneous and inhomogeneous bundles of single-walled carbon nanotubes. Journal of Physics: Condensed Matter. 2009;**21**(4):045302. DOI: 10.1088/0953-8984/21/4/045302

[51] Okada S. Radial-breathing mode frequencies for nanotubes encapsulating fullerenes. Chemical Physics Letters. 2007;**438**:59-62. DOI: 10.1016/j.cplett.2007.02.058

[52] Snoke DW, Cardona M. A bond polarizability model for the C_{60} Raman spectrum. Solid State Communications. 1993;**87**(2):121-126. DOI: 10.1016/0038-1098(93)90339-O

[53] Lynch K, Tanke C, Menzel F, Brockner W, Scharff P, Stumpp E. FT-Raman spectroscopic studies of C_{60} and C_{70} subsequent to chromatographic separation including solvent effects. Journal of Physical Chemistry A. 1995;**99**:7985-7992. DOI: 10.1021/j100020a022

[54] Wang KA, Zhou P, Rao AM, Eklund PC, Jishi RA, Dresselhaus MS. Intramolecular-vibrational-mode softening in alkali-metal-saturated C_{70} films. Physical Review B. 1993;**48**: 3501-3506. DOI: 10.1103/PhysRevB.48.3501

[55] Bethune DS, Meijer G, Tang WC, Rosen HJ, Golden WG, Seki H, Brown CA, Vries MS. Vibrational Raman and infrared spectra of chromatographically separated C_{60} and C_{70} fullerene clusters. Chemical Physics Letters. 1991;**179**:181-186. DOI: 10.1016/0009-2614(91)90312-W

[56] Gallagher SH, Bolskar RD, Lay PA, Reed CA. Raman excitation profiles of C_{70} in benzene solutions. Assignment of electronic spectrum in the 380-510 nm region. Journal of the American Chemical Society. 1997;**119**:4263-4271. DOI: 10.1021/ja963426f

[57] Sun G, Kertesz M. Vibrational Raman spectra of C_{70} and studied by density functional theory. Journal of Physical Chemistry A. 2002;**106**:6381-6389. DOI: 10.1021/jp020222e

IntechOpen